Zero-Field Slow Magnetic Relaxation and Hysteresis Loop in Four-Coordinate Co^{II} Single-Ion Magnets with Strong Easy-Axis Anisotropy

Hui-Hui Cui,[a] Fang Lu,[b] Xue-Tai Chen,*[a] Yi-Quan Zhang,*[b] Wei Tong,[c] and Zi-Ling Xue[d]

[a]*State Key Laboratory of Coordination Chemistry, School of Chemistry and Chemical Engineering, Nanjing University, Nanjing 210023, China*

[b]*Jiangsu Key Laboratory for NSLSCS, School of Physical Science and Technology, Nanjing Normal University, Nanjing 210023, China*

[c]*Anhui Province Key Laboratory of Condensed Matter Physics at Extreme Conditions, High Magnetic Field Laboratory of the Chinese Academy of Science, Hefei 230031, Anhui, China.*

[d]*Department of Chemistry, University of Tennessee, Knoxville, Tennessee 37996, USA*

Abstract: Two mononuclear tetrahedral Co(II) complexes $(HNEt_3)_2[Co(L^1)_2]\cdot H_2O$ (**1**) and $(Bu_4N)_2[Co(L^2)_2]\cdot H_2O$ (**2**) (H_2L^1 = *N*,*N*'-bis(p-toluenesulfony1)oxamide, H_2L^2 = *N*,*N*'-diphenyloxamide) have been synthesized and their structures have been characterized by single-crystal X-ray diffraction. Both complexes adopt distorted tetrahedral coordination geometries surrounding the Co(II) center, which is ligated by two doubly deprotonated oxamide ligands oriented perpendicularly to each other. Their highly axial magnetic anisotropies were revealed by the direct current (dc) magnetic measurements, high-field and high-frequency electron paramagnetic resonance (HFEPR) and theoretical calculations. Both complexes display slow magnetic relaxation in the absence of an applied dc field. Upon application of the 0.15 T dc field, the quantum tunneling of magnetization (QTM) has been suppressed efficiently. In addition, both complexes display hysteresis loops with different field sweep rates at 1.8 K, which is rarely observed for Co(II) single-ion magnets (SIMs).

Introduction

Since the first observation of slow magnetic relaxation and hysteretic effect in polynuclear metal complexes in 1993,[1] single-molecule magnets (SMMs)[2] have aroused great attention due to their potential applications in high-density information storage of digital data, quantum computations and spintronics devices.[3] Such complexes usually possess long spin relaxation times because of a high energy barrier to spin inversion arising from the presence of strong magnetic anisotropy. The effective energy barrier U_{eff} is defined as $U_{eff} = |D|S^2$ for the molecules with integer spin ground state and $U_{eff} = |D|(S^2 - 1/4)$ for those with half-integer spin ground state, where D is the axial zero-field splitting (ZFS) parameter and S represents

the spin of the ground state. Importantly, it has been proved difficult to enhance the energy barrier only by increasing the spin of the ground state in mostly polynuclear coordination complexes of first row transition metals since the *D* value will go down with increasing the value of *S*.[4] Hence the attention has subsequently turned to the ions with strong magnetic anisotropy. In 2003, the discovery of slow magnetic relaxation in mononuclear rare-earth complexes refreshed the area of SMM.[5] Similar SMM behavior was subsequently observed on mononuclear transition metal compounds by Freedman and coworkers in 2010.[6a] Since the slow magnetic relaxation comes from a single magnetic metal center in these complexes, they are referred to as single-ion magnets (SIMs), which are the simplest system of SMMs. SIMs are particularly attractive because their magnetic anisotropy and slow magnetic relaxation could be modified properly by structural modulation. The dynamic behavior would depend on the coordination environment around the metal center. Even small structural changes may make a significant impact on the nature and magnitude of magnetic anisotropy.

Since the first discovery of the 3d-SIM,[6a] more and more SIMs based on first-row transition metal ions have been reported, and the number is rapidly increasing.[7] A particular attention has been paid to the Co^{II}-based complexes due to its strong spin-orbit coupling and the half-integer spin. A large number of Co^{II}-based SIMs in various coordination environments along with the coordination number from two to eight have been reported.[8-14] However, only few of them exhibit slow magnetic relaxation in the absence of a dc field while the majority are field-induced SIMs, in which a dc magnetic field is needed to suppress effectively the fast relaxation through quantum tunneling of magnetization (QTM).[15]

Tetrahedral Co(II) complexes are especially important for the design of Co(II)-based

SIMs because they are normally air- and moisture-stable compared with those low coordinated Co(II) complexes, which could possess high energy barrier.[8] The majority of the reported four-coordinate Co(II)-SIMs are composed of mixed donor sets[9] while relatively few are known to contain the four identical donors with the CoX_4 moiety (X = O, S, Se, Te,[10] N[11], Cl[12]). Those with large *D* values ($|D| > 50$ cm^{-1}) and high relaxation energy barriers U_{eff} ($U_{eff} > 30$ cm^{-1}) are summarized in Table S1 (Supporting Information).[10c-d,11b-c] These complexes usually exhibit the zero-field slow magnetic relaxation. It should be noted that they all bear four identical donors such as S and N atoms. Two complexes bearing *N,N'*-chelating ligands (Chart 1), i.e., $(HNEt_3)_2[Co(pdms)_2]$ and $[Co\{NtBu)_3SMe\}_2]$, show the hysteresis loop observed by using a commercially available standard Quantum Design SQUID magnetometer.[11b,c] It is reasoned that fine-tuning of the geometric distortion and electronic structure of the tetrahedral Co(II) complexes with four identical donors would promote large easy-axis anisotropy and magnetic dynamic properties.

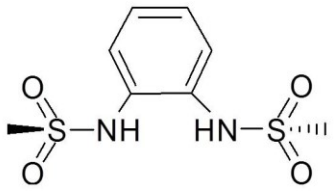

H_2(pdms)

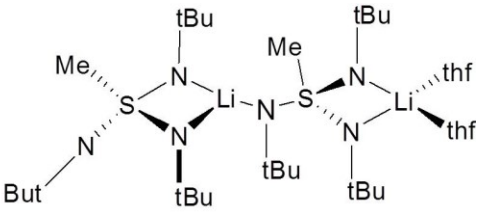

$[(thf)_2Li_2\{(NtBu)_3SMe\}_2]$

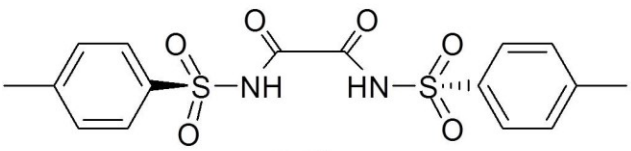

H_2L^1

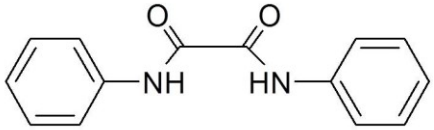

H_2L^2

Chart 1. *N,N'*-chelating ligands of H_2(pdms), $[(thf)_2Li_2\{(NtBu)_3SMe\}_2]$, H_2L^1 and H_2L^2.

In the current work, we employed the *N,N'*-chelating oximide ligands, L^1 and L^2 (H_2L^1 =

N,*N*'-bis(p-toluenesulfony1)oxamide, H_2L^2 = *N*,*N*'-diphenyloxamide, Chart 1), to prepare the mononuclear Co(II) complexes with two aims. First, the oximides could have similar chelating angles and two negative charges with $pdms^{2-}$, which could give similar magnetic anisotropy. Second, the bridging capability of the oximides would make the resulting mononuclear complexes as very promising building blocks to construct the one-dimensional complexes or polynuclear clusters in the future work. Herein, we report two mononuclear tetrahedral Co(II) complexes $(HNEt_3)_2[Co(L^1)_2]\cdot H_2O$ (**1**) and $(Bu_4N)_2[Co(L^2)_2]\cdot H_2O$ (**2**), which have been intensively studied by the X-ray structure analyses, HFEPR spectroscopy, magnetic measurements and theoretical calculations. The oxamide ligands introduce serious structural distortions, resulting in a large and negative single-ion magnetic anisotropy required for single-molecule magnet properties. Slow magnetic relaxation at zero external magnetic field was observed for these two complexes. The presence of the hysteresis loop of the magnetization with different sweep rates at 1.8 K is very rare for a Co(II) SIMs.[8a,8b,11b-c,13g,h]

Experimental Section

General Characterization and Physical Measurements.

All experiments were carried out under dry nitrogen atmosphere by using standard Schlenk techniques. Solvents were dried by conventional methods prior to use. All other chemicals were employed from commercial sources and were used without further purification, except that *N*,*N*'-bis(p-toluenesulfony1)oxamide (H_2L^1) and *N*,*N*'-diphenyloxamide (H_2L^2) were synthesized according to the literature methods.[16-17] Powder X-ray diffraction (PXRD)

patterns were recorded on a Bruker D8 ADVANCE X-ray powder diffractometer equipped with a Cu Kα X-ray radiation (λ = 1.54056 Å) over the 2θ range of 5°-50° at room temperature. Elemental analyses (C, H and N) were carried out on an Elementar Vario ELIII elemental analyzer. IR spectra were recorded on a FT-IR spectrometer (Vector 22) spectrometer with KBr pellets in the 400-4000 cm^{-1} region. Solid UV-Vis-NIR spectra were measured as diffuse reflectance on polycrystalline powders of **1** and **2** using a Varian Cary 5000 spectrophotometer in the 4000 to 30000 cm^{-1} region at room temperature.

Synthesis of $(HNEt_3)_2[Co(L^1)_2]\cdot H_2O$ (1). $CoCl_2$ (0.5 mmol, 0.065 g) and H_2L^1 (1.0 mmol, 0.397 g) were dissolved in 30 mL of mixed solvents (15 mL CH_2Cl_2 and 15 mL CH_3OH). NEt_3 (3 mL) was added to the above solution. The color of the reaction mixture changed immediately from blue to red violet. The reaction mixture was stirred at room temperature for another 3 h and then diethyl ether (80 mL) was added. The resulting red violet precipitate was collected and then dissolved in 15 mL of acetonitrile. Diffusion of diethylether into the acetonitrile solution yielded pink crystals with a yield of 70% based on Co. Anal. Calc. for $C_{44}H_{62}CoN_6O_{13}S_4$: C, 49.38; H, 5.84; N, 7.85. Found: C, 49.36; H, 5.83; N, 7.86.

Synthesis of $(Bu_4N)_2[Co(L^2)_2]\cdot H_2O$ (2). Bu_4NOH (3 mL, 40% in CH_3OH) was added to a solution of H_2L^2 (1.0 mmol, 0.25 g) in 10 mL of DMF. The mixture was stirred until the solution was clear. Then $CoCl_2\cdot 6H_2O$ (0.5 mmol, 0.119 g) was added. After stirring at room temperature for another 6 h, diethyl ether (100 mL) was added. The resulting red precipitate was collected and then dissolved in 15 mL of acetonitrile. Diffusion of diethylether into the acetonitrile solution yielded red crystals with a yield of 60% based on Co. Anal. Calc. for $C_{60}H_{94}CoN_6O_5$: C, 69.40; H, 9.12; N, 8.09. Found: C, 69.46; H, 9.18; N, 7.99.

X-ray Single-Crystal Structure Determination. Suitable single crystal of **1** or **2** was selected from the mother liquor and covered with paraffin liquid. Single-crystal X-ray diffraction experiments were carried out at 155 K on a Bruker APEX DUO diffractometer equipped with a CCD area detector using graphite-monochromated Mo Kα radiation (λ = 0.71073 Å).[18] A hemisphere of data were collected using a narrow-frame method with an exposure time of 1 s for **1** and 3s for **2** per frame. The APEXII program was used to determined unit cell parameters. The data were integrated with SAINT program,[19] which were corrected for Lorentz factor and polarization effects. And the multiscan absorption corrections were applied using SADABS.[20] The molecular structures were solved and refined via full-matrix least-squares on F^2 using SHELX program (version 2014/7).[21] All non-hydrogen atoms were refined with anisotropic displacement parameters while the hydrogen atoms were refined isotropically on calculated positions, with the vibration parameters related to the corresponding non-hydrogen atoms. Crystal data and the final refinement parameters of the studied complexes are shown in Table S2. Additional refinement details of two compounds were recorded in the corresponding CIF file (see Supporting Information).

Magnetic Measurements. Magnetic measurements were performed on a vibrating sample magnetometer (VSM) of Quantum Design MPMS SQUID-VSM system. Measurements for two complexes were performed on finely ground microcrystalline powders, which were restrained in a frozen eicosane matrix and tightly packed in a polycarbonate plastic capsule to prevent torquing of crystallites in magnetic fields. Direct current (dc) magnetic susceptibilities were measured in the dc mode of detection with an applied field of 0.1 T in

the temperature range 2−310 K. The magnetization data were taken up to 7 T under different temperatures. The magnetic susceptibilities data were corrected for the diamagnetic contributions of samples as well as for the background of the eicosane using Pascal's constants.[22] The alternating current (ac) susceptibility data were obtained with a 0.2 mT ac field oscillating at frequencies of 1−1000 Hz under different applied dc fields and temperatures.

High-field and high-frequency electron paramagnetic resonance (HFEPR) measurement. HFEPR data was collected on a home-built multi-frequency high-field electron magnetic resonance spectrometer at Chinese High Magnetic Field Laboratory, Hefei. Measurements were performed on ground powders immobilized with eicosane and pressed tightly to minimize the effect of field-induced torquing.

Results and Discussion

Synthesis and Characterization. Complexes **1** and **2** were synthesized by the reactions of H_2L^1/H_2L^2 and $CoCl_2$/$CoCl_2 \cdot 6H_2O$ with molar ratio of 2:1 in methanol/dichloromethane or DMF at room temperature (Scheme 1). Excess NEt_3 or Bu_4NOH was used as a base. Plenty of diethylether was added to the reaction mixture to deliver the brightly colored solid, which was subsequently dissolved in a moderate amount of acetonitrile. The single crystals suitable for X-ray diffraction were obtained by the slow diffusion of diethylether into the acetonitrile solution. The phase purity of the crystals was confirmed by the powder X-ray diffraction (PXRD), which agrees well with those simulated by the single crystal X-ray data (Figures S1-S2).

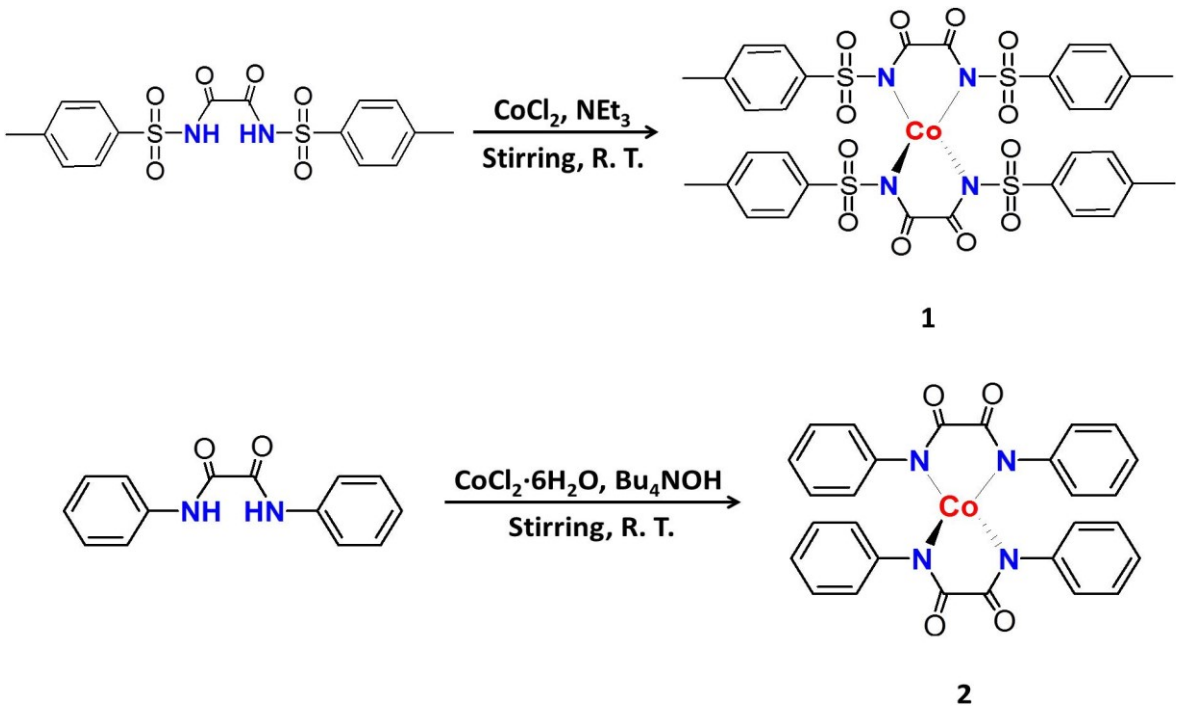

Scheme 1. Synthetic routes to 1 and 2.

Both complexes were characterized by IR and solid UV-Vis-NIR diffuse reflectance spectra. The IR spectra revealed a strong absorption band at the 1671 cm^{-1} for **1** and 1666 cm^{-1} for **2**, in the range of 1630-1680 cm^{-1} typical for the band of C=O groups,[23] which are assigned to the C=O groups in oxamide ligands (Figure S5).

In the solid UV-Vis-NIR diffuse reflectance spectra of **1** and **2** (Figure S6), there are three obvious absorption bands in the record region of 4000-30000 cm^{-1}. The strong absorption above 25000 cm^{-1} is attributed to ligand-based transitions or charge-transfer transitions between metal ion and ligands. Two other bands are clearly observable between 5000 and 25000 cm^{-1}. Besides, there is one weak band observed below 5000 cm^{-1}, which is on the low bound of the energy range. In an idealized T_d symmetry, three spin-allowed transitions are expected: $\nu_1 = {}^4A_2\,({}^4F) \rightarrow {}^4T_2\,({}^4F)$, $\nu_2 = {}^4A_2\,({}^4F) \rightarrow {}^4T_1\,({}^4F)$ and $\nu_3 = {}^4A_2\,({}^4F) \rightarrow {}^4T_1\,({}^4P)$ in an increasing order of energy.[24] The band below 5000 cm^{-1} is assigned as the ν_1 transition while

those observed in NIR region (5000-13000 cm^{-1}) and the visible region (15000-24000 cm^{-1}) refers to the ν_2 and ν_3 transitions, respectively. The absorption envelopes display multiple bands and broadness possibly resulting from spin−orbit coupling and/or structural distortions from ideal tetrahedral geometry. Since the energy of the ν_1 transition is not easily determined due to their weak appearance. From the average energies of the other two bands (ν_2 = 8060 and ν_3 = 18281 cm^{-1} for **1** and ν_2 = 8273 and ν_3 = 17988 cm^{-1} for **2**), the tetrahedral crystal field splitting (10*Dq*) and the Racah parameter (*B*) can be calculated[25] to be *Dq* = 467 cm^{-1} and *B* = 822 cm^{-1} for **1** and *Dq* = 482 cm^{-1} and *B* = 787 cm^{-1} for **2**. Accordingly the transition ν_1 is expected to be 10*Dq*, *i.e.* 4670 cm^{-1} for **1** and 4820 cm^{-1} for **2**, which are consistent with the relatively weak bands below 5000 cm^{-1} in Fig. S5.

Structural Descriptions. As illustrated in Table S2, complex **1** crystallizes in orthogonal space group $P2_12_12_1$ with four molecules in the unit cell, while **2** crystallizes in triclinic space group $P\bar{1}$ with two molecules in the unit cell. The selected bond lengths and bond angles are listed in Table 1. Single crystal X-ray diffraction studies of both complexes reveals a distorted tetrahedral coordination geometry surrounding the Co(II) center, which is ligated by two doubly deprotonated oxamide ligands oriented perpendicularly to each other (Figure 1). The overall two negative charge of the anion is neutralized by two $NHEt_3^+$ cations for **1** and two Bu_4N^+ cations for **2**. The structure of a similar Co(II) complex has been deposited in CCDC with number 247784.[26] The Co–N bond lengths are very similar in **1** (1.988(5)-2.005(5) Å) and **2** (1.984(3)-1.987(3) Å). But the average Co−N bond length of **1** (1.994 Å) is slightly longer than that of **2** (1.988 Å). The N-Co-N angles in both complexes can be classified into two categories. Two smaller N-Co-N angles are 81.7(2)°, 81.3(2)° for **1**

and 83.38(12)°, 84.78(12)° for **2** due to the chelation of oxamide ligands. The other four larger N-Co-N angles are in the range of 121.7(2)°-127.6(2)° in **1** and 120.88(13)°-125.07(12)° in **2**. These deviate seriously from the ideal angle of 109.5° for a perfect tetrahedron. Therefore, the structure of **1** prefers a more elongated tetrahedron than **2**. The two coordination planes defined by the Co-N-C-C-N metallacycles are almost perpendicular with an angle of 86.68(6)° for **1** and 85.37(3)° for **2** (Figures S3-S4).

The bulky peripheral substituents and cations make the central Co(II) ions well isolated from each other. The closest intermolecular Co---Co distances are relatively long with 11.37(2) Å for **1** and 10.39(4) Å for **2**, making the contact among the neighboring molecules negligible. No other interaction like hydrogen bond was observed except for van der Waals' forces in the crystal lattice for both complexes. The continuous shape measure (CSM) analyses have been calculated with SHAPE software[27] to evaluate the degree of deviation from the ideal tetrahedron. The distortion values are 5.89 and 4.86 for **1** and **2**, respectively (Table S3), indicating that the molecular geometries of **1** and **2** deviate distantly from the ideal tetrahedron.

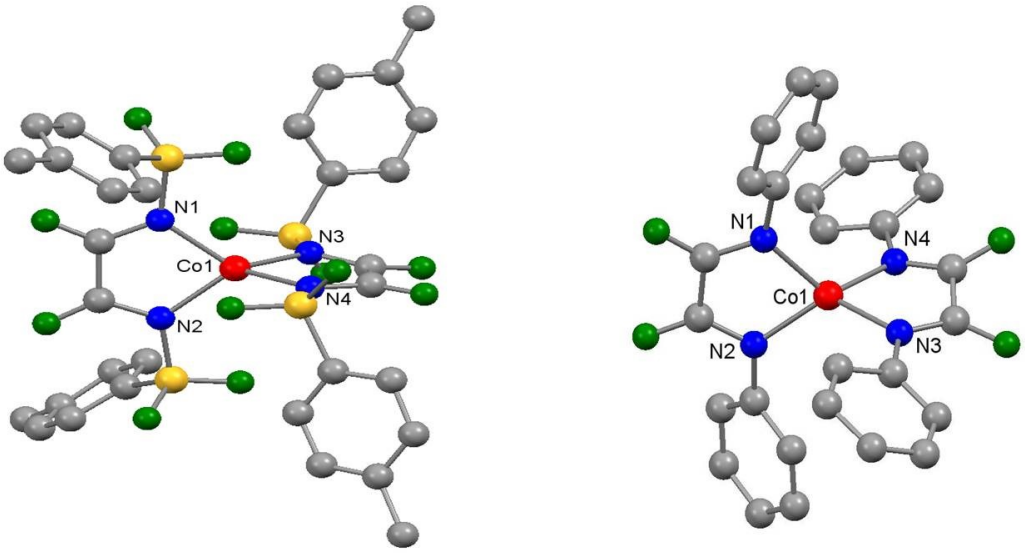

Figure 1. Crystal structure of the anions of **1** and **2**. Co is shown in red, N in blue, O in green, S in yellow, and C in grey. H atoms have been omitted for clarity.

Table 1. Selected Bond Lengths (Å) and Angles (deg) for 1 and 2

1		**2**	
Co1-N1	1.988(6)	Co1-N1	1.984(3)
Co1-N2	2.005(5)	Co1-N2	1.987(3)
Co1-N3	1.996(5)	Co1-N3	1.990(3)
Co1-N4	1.988(5)	Co1-N4	1.992(3)
N1-Co1-N2	81.7(2)	N1-Co1-N2	83.38(12)
N3-Co1-N4	81.3(2)	N3-Co1-N4	84.78(12)
N1-Co1-N3	127.6(2)	N1-Co1-N3	124.50(12)
N2-Co1-N4	125.5(2)	N2-Co1-N4	125.07(12)
N1-Co1-N4	125.4(2)	N1-Co1-N4	120.88(13)
N2-Co1-N3	121.7(2)	N2-Co1-N3	123.43(13)

Magnetic Anisotropy. Magnetic static properties of **1** and **2** have been studied by dc magnetic measurements, HFEPR and theoretical calculations. Variable-temperature dc magnetic susceptibilities were measured on polycrystalline powders of **1** and **2** at an applied dc field of 0.1 T between 1.8 and 300 K (Figures 2 and S7). The room temperature magnetic susceptibility-temperature products, $\chi_M T$, are 3.19 and 3.21 $cm^3\ mol^{-1}$ K for **1** and **2**, respectively, corresponding to the expected value for an $S = 3/2$ ion with $g = 2.61$ and 2.62. These large observed $\chi_M T$ values are much higher than the spin-only value of 1.875 $cm^3\ mol^{-1}$ K expected for a $S = 3/2$ system ($g = 2.0$), indicating a sizable contribution of orbital angular momentum. **1** and **2** exhibit similar trend in the $\chi_M T$–T plots. With decreasing temperature, the $\chi_M T$ values remains constant until 150 K, below which they decrease rapidly to 2.61 and 2.52 $cm^3\ mol^{-1}$ K at 2 K for **1** and **2**, respectively. The sudden drop of the $\chi_M T$ value suggests the presence of a large zero-field splitting rather than the intermolecular interactions, because the nearest Co–Co distance is so large.

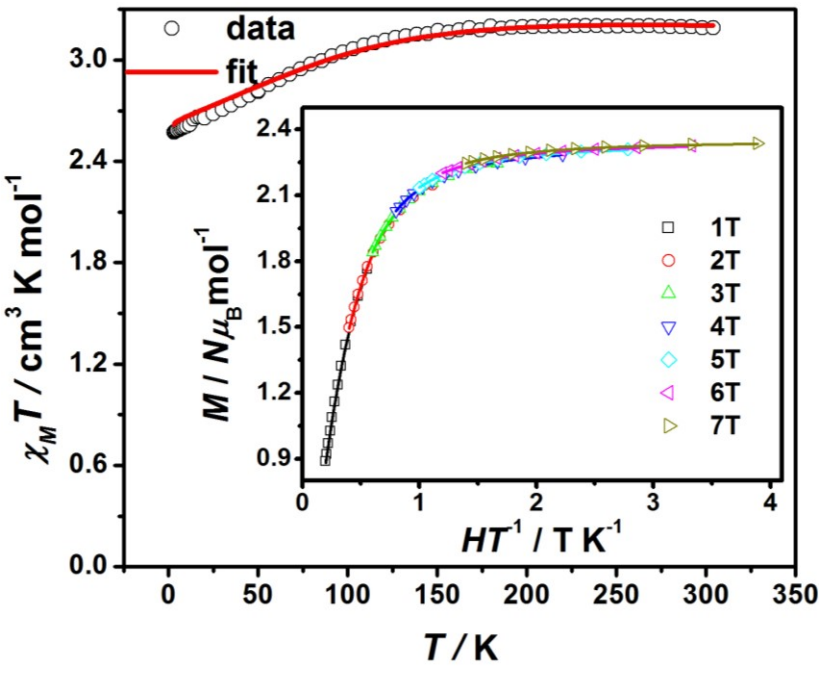

Figure 2. Variable-temperature dc susceptibility data recorded on a powder sample of **1** at an applied field of 0.1 T. Inset: Variable-temperature, variable-field dc magnetization data of **1**. The solid line is the fit to the experimental data with the program *PHI*.[28]

The large magnetic anisotropy is further confirmed by the magnetization (*M*) versus *H* plots, which were recorded at 1.8 K up to 7 T (Figure S8). As the applied dc field increases, the magnetization rises gradually to 2.44 and 2.40 $N_A\mu_B$ for **1** and **2** at 7 T, respectively, which are far below the expected saturation value (3 $N_A\mu_B$), suggesting the presence of magnetic anisotropy. Low-temperature magnetization data from 1.8 to 5.0 K at various applied dc fields were also measured for **1**-**2.** Although the resulting *M* vs *H/T* plots (Figures 2 and S9) exhibit the superimposition of the iso-field curves, they are attributed to a large magnetic anisotropy, which has been reported in the literatures.[11b,13e,f]

For tetrahedral Co(II) complexes, the d^7 ground term is $^4A_2$ in ideal T_d symmetry, meaning the first-order orbital angular momentum has been quenched. Thus, tetrahedral Co(II) ion is usually assumed to be a pure spin ion. The static magnetic properties of nearly all reported mononuclear tetrahedral Co(II) complexes have been modelled via the spin-Hamiltonian.[9-12] Accordingly, the experimental $\chi_M T$ vs *T* and *M* vs *H/T* curves of **1** and **2** were fit simultaneously by the *PHI* program[28] using a conventional spin Hamiltonian for an $S = 3/2$ system with zero-field splitting and Zeeman effect, considering anisotropic parameters ($g_x = g_y$) as given in eqn. 1:

$$H = D(\hat{S}_z^{\,2} - S(S+1)/3) + E(\hat{S}_x^{\,2} - \hat{S}_y^{\,2}) + \mu_B g\hat{S}\cdot H \qquad (1)$$

The parameters D and E are the axial and rhombic anisotropy parameters, S are the spin operator, μ_B is the Bohr magneton, g is a tensor and H are the magnetic field vector, respectively. The data were fitted well with D = -144.1(3) cm^{-1}, E = 0.02(7) cm^{-1}, $g_x = g_y$ = 2.2(2), g_z = 3.0(3) for **1** and D = -130.8(9) cm^{-1}, E = -0.70(0) cm^{-1}, $g_x = g_y$ = 2.2(7), g_z = 3.0(2) for **2**. For both complexes, the signs of ZFS parameters D are negative and the ratio of $|E/D|$ are relatively small, indicating that these complexes exhibit easy axis anisotropy with the ground state $M_S = \pm 3/2$ being the lowest in energy. The D values of **1** and **2** are among the largest ones reported for the four-coordinate Co(II) complexes (Table S1).[10c-e,11b-c]

Considering the strong distortion of **1** and **2** with respect with the tetrahedral geometry, their electronic structures have been studied by ab initio theoretical calculations. The XMS-CASPT2[29] calculations considering the effect of the dynamic electron correlation based on complete-active-space self-consistent field (CASSCF) method were performed on the basis of X-ray determined geometries of **1** and **2** (Figure S10) using MOLCAS 8.2 program package.[30] Calculation details are given in Supporting Information. The calculated energies (cm^{-1}) of the lowest ten spin-free terms and the lowest two spin-orbit states for **1** and **2** are shown in Tables S4-S5. The energy differences between the lowest two spin-free states are 240.057 cm^{-1} for **1** and 117.905 cm^{-1} for **2**, which are smaller than those between the lowest two spin-orbit states (261.7 cm^{-1} for **1** and 289.8 cm^{-1} for **2**, Table S5). Moreover, the ground spin-orbit states of **1** and **2** are not only from the ground spin-free state, but also from the first excited one (Table S5). The lowest energy gap between the lowest two spin-free states (240.057 cm^{-1} for **1** and 117.905 cm^{-1} for **2**) is of the size of the spin-orbit coupling constant (ξ_{eff} = 446 cm^{-1}).[11c] These results strongly suggest a quasi-degeneracy of the multielectron

ground and the first excited states. Such a quasi-degeneracy suggests that spin-Hamiltanian based on the perturbation theory should not be used in the evaluation of magnetic anisotropy parameters such as *g, D* and *E*. Therefore *D* and *E* values derived from the above fitting of the magnetic data by eqn. 1 can be false. They should be regarded to be qualitative as suggested for the tetrahedral complex $(HNEt_3)_2[Co(pdms)_2]$.[11c]

The calculated effective *g*-values corresponding to the fictitious spin $S = 1/2$ of the ground state Kramers doublet of **1** and **2** are also shown in Table S6, where the ground state $g_x = 0.099$, $g_y = 0.104$ and $g_z = 9.758$ for **1** and $g_x = 0.018$, $g_y = 0.018$ and $g_z = 9.823$ for **2**. These axial anisotropy of *g* values suggests the highly axial magnetic anisotropy in **1** and **2**. With the smaller g_x and g_y values, the quantum tunneling of magnetization (QTM) in the ground state induced by transversal magnetic field ($2\Delta_{tun} = \mu_B[g_x^2H_x^2 + g_y^2H_y^2]^{1/2}$) can be suppressed effectively,[31] which is consistent with the observed zero-field slow magnetic relaxation and hysteresis loop (see below).

Furthermore, the calculated $\chi_M T$ versus T plots of **1** and **2** are shown in Figure S11 and the calculated field dependence of magnetizations under low temperature are shown in Figure S12, in which all the calculated data conform well to the experimental ones. The calculated orientations of the g_x, g_y, g_z in the ground spin-orbit state on Co^{II} ion of **1** and **2** are shown in Figure S13. Just like other elongated tetrahedral Co(II) complexes,[10d,11c] the magnetic axis lies in the C_2 axis going through the midpoints of backbone of oxamide ligands.

In order to further confirm the axial magnetic anisotropies of **1** and **2**, HFEPR spectra were recorded on polycrystalline samples of **1** and **2** with different frequencies (Figures S14-S15). There is no obvious HFEPR signal observed for **1** and **2.** Such "EPR-silent"

behaviour in a high-spin Co(II) system[24a] could occur only in the case when the $Ms = \pm 3/2$ Kramers doublet lies at lower energy than the $Ms = \pm 1/2$ doublet, corresponding to easy-axis magnetic anisotropy. The intra-Kramers EPR transition within the ±3/2 doublet corresponding to $\Delta Ms = \pm 3$ is nominally forbidden. The transition could be partly allowed when a sizable rhombic ZFS *E*-term mixes the ±3/2 doublet with the ±1/2 doublet. The absence of HFEPR signal in **1** and **2** suggests that the magnetic anisotropy is nearly axial, in consistent with the calculation results.

Dynamic Magnetic Properties. To investigate the magnetic relaxation dynamics, frequency- and temperature-dependent alternating current (ac) susceptibility measurements were performed on polycrystalline samples of **1** and **2** in the frequency range of 1−1000 Hz. The ac magnetic susceptibility data were found to show significant frequency-dependence of both in-phase (χ_M') and out-of-phase (χ_M'') susceptibilities even without the application of a static external field, indicating a slowly relaxing magnetic moment (Figures 3 and S16–S18). Thus, **1** and **2** display zero-field slow magnetic relaxation, which is rarely observed in Co(II)-SIMs.[8a,8b,9b-c,10,11] As shown in Figures 3 and S18, both in-phase (χ_M') and out-of-phase (χ_M'') susceptibilities show frequency-dependence in a broad temperature range. For **1** and **2**, the maximum appears at $\nu = 1.0$ Hz and decreases in height with increasing temperature, but at the same time the peak shifts to higher frequency. Furthermore, the signals at all different frequencies show strong upturn at low temperature, which could be due to the impact of quantum tunneling of magnetization (QTM) on the relaxation process. Such influence caused by QTM has been found in other Co(II)-SIMs.[10d,13f] In order to reduce the effect of QTM, a dc field of 0.15 T was applied for both complexes to measure the ac susceptibilities (Figures

3 and S19-S21). Obviously, the upturn at low temperature has diminished dramatically, indicating that QTM has been suppressed efficiently. Interestingly, the frequency dependent out-of-phase ac susceptibilities at 0 T reveal a second relaxation pathway under low temperatures below 4.5 K and low frequencies below 10 Hz for both complexes (Figures S16-S17). In contrast, there was only one relaxation process when a dc field of 0.15 T was applied for both complexes (Figure S19-S20). This second relaxation pathway is the same as the upturn observed in temperature dependence of in-of-phase (χ_M') and out-of-phase (χ_M'') ac susceptibility shown in Figure 3, which is due to the impact of QTM.[6b]

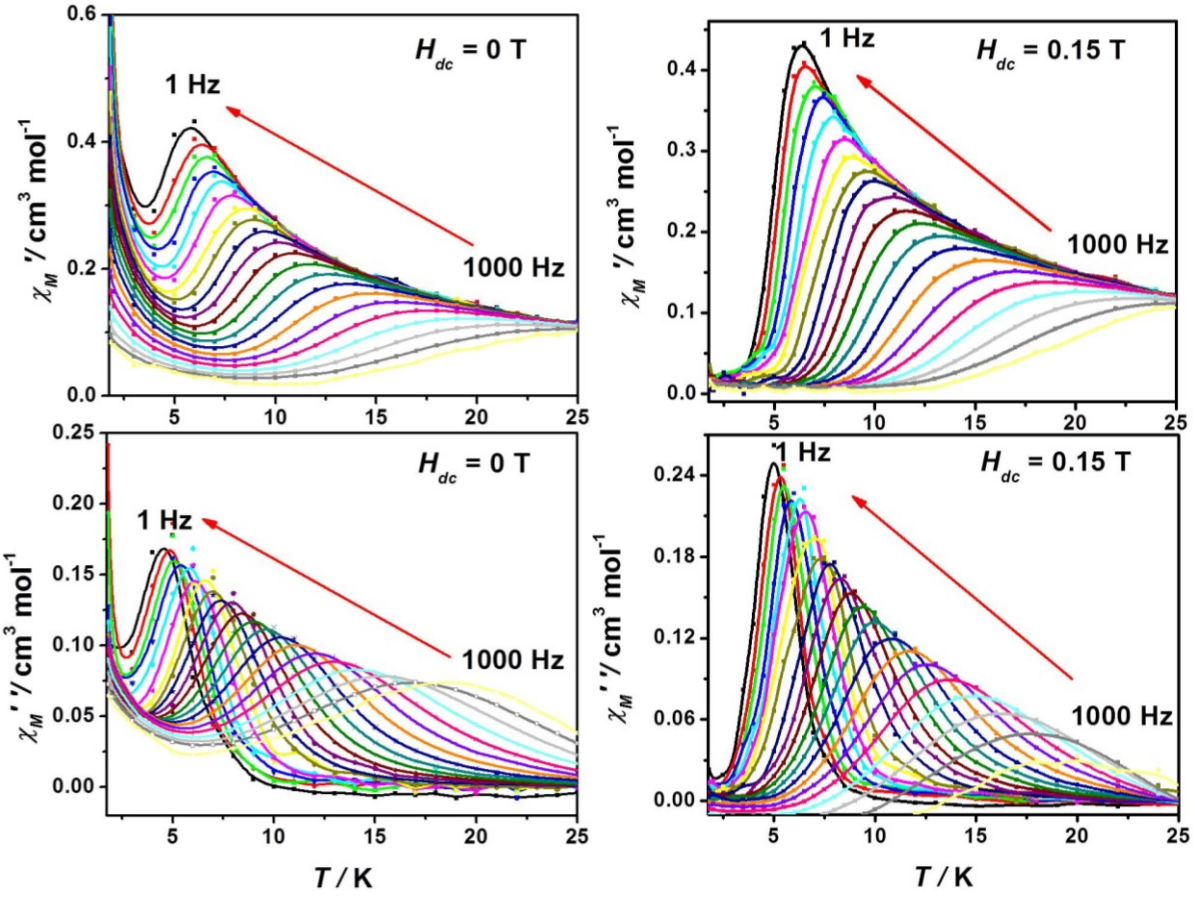

Figure 3. Temperature dependence of in-of-phase (χ_M') and out-of-phase (χ_M'') ac susceptibility for **1** at different ac frequency under zero field and 0.15 T dc field.

The plots of ln(τ) *vs* T^{-1} were extracted from the peak values of the variable-frequency susceptibility data under the zero filed (Figures S17-S18) to give magnetic relaxation times (τ). Assuming the Orbach process occurring at high temperature range, linear fit to the five data points in the high temperature region according to the Arrhenius law $\tau = \tau_0 \exp(U_{eff}/kT)$ gave U_{eff} = 46.02 cm^{-1} with τ_0 = 5.40 × 10^{-6} s for **1** and U_{eff} = 58.41 cm^{-1} with τ_0 = 2.47 × 10^{-6} s for **2**, respectively (Figure 4a and S22). However, the resulting energy barriers are much smaller than the calculated energy gap between the lowest two spin-orbit states (261.7 cm^{-1} for **1** and 289.8 cm^{-1} for **2**). This is perhaps not surprising, as the estimation of effective energy barrier here is based on the assumption of an Orbach process as dominant relaxation processes in the high-temperature range. It has been showed that the Orbach mechanism is not necessarily the dominant pathway at least in the studied temperature range. ~~The above estimation of energy barrier for the Orbach process is incorrect.~~ The curvature in the Arrhenius plots of **1** and **2** implies a non-negligible direct and/or Raman processes in determining the relaxation rate. Thus, we tried to fit the relaxation times with a multi-processes, given by eqn. 2,[32]

$$\tau^{-1} = AT + CT^n + \tau_0^{-1} exp\left(-U_{eff} / kT\right) \qquad (2)$$

where the first, second and third term represents direct process, Raman process and Orbach process, respectively.[33] Many attempts showed that only Raman process was utilized to fit the data because no reasonable agreement could be obtained when considering other processes simultaneously. The best fit by a power law $\tau^{-1} = CT^n$ is obtained with C = 0.004(1) s^{-1} K$^{-4.8}$, n = 4.8(7) for **1** and C = 0.01(3) s^{-1} K$^{-4.3}$, n = 4.3(3) for **2**, suggesting a dominant Raman-like

process in the studied temperature range (Figures 4a and S22).

The relaxation times of **1** and **2** obtained at the different times under 0.15 T field were similarly extracted. A comparison of the relaxation times under zero and 0.15 T shows that the relaxation times do not display the dramatic field-dependence in the whole temperature range (Figure S23). The relaxation times were reasonably fitted by a power law $\tau^{-1} = CT^n$ to give $C = 0.01(1)$ s^{-1} $K^{-4.3}$, $n = 4.3(7)$ for **1** and $C = 0.01(0)$ s^{-1} $K^{-4.3}$, $n = 4.3(8)$ for **2** (Figure S24). Again, these results showed that the Raman mechanism is the dominant process at zero field and 0.15 T in the studied temperature range in **1** and **2**. The contribution of other processes including the Orbach process can be neglected.

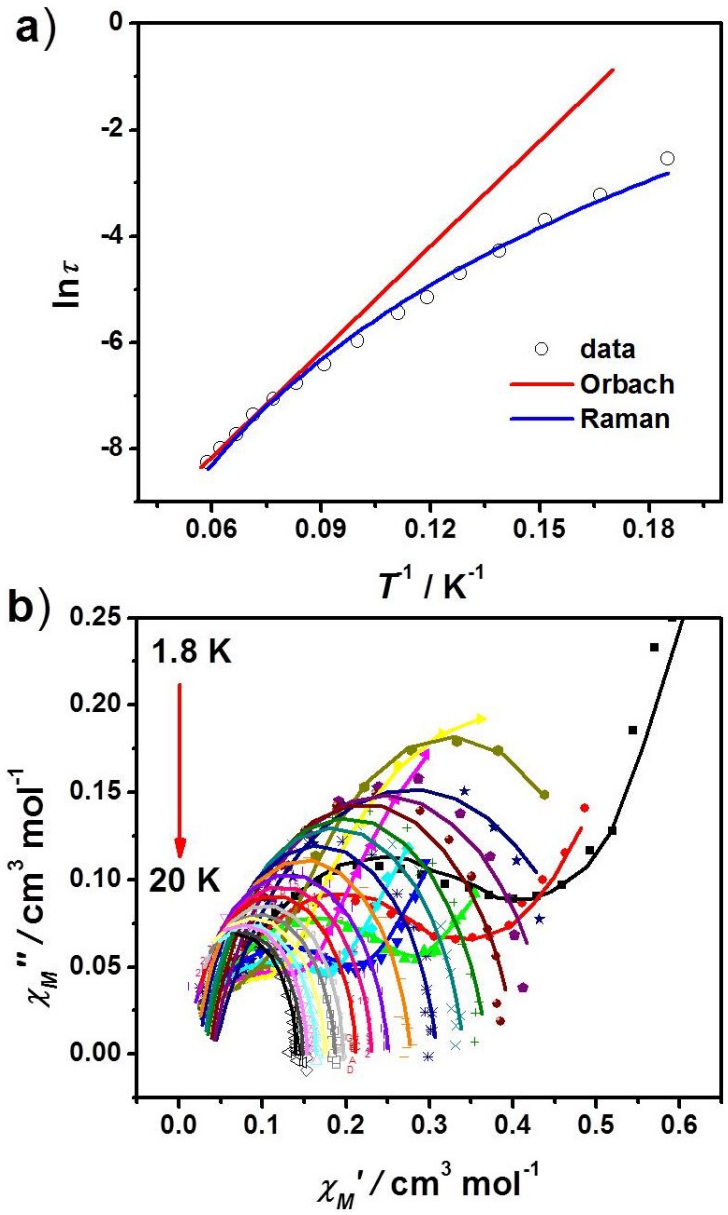

Figure 4. (a) Relaxation time of the magnetization *ln(τ)* vs T^{-1} plots for **1** under zero dc field. The red line represents the best fit by the Arrhenius law $\tau = \tau^0 \exp(U_{eff}/k_BT)$ and the blue line represents the best fit by the Raman process with $\tau^{-1} = CT^n$. (b) Cole−Cole plots for **1** under zero dc field. The solid lines are the best fits to the experiments with the generalized Debye model.[33]

The χ_M'' vs. χ_M' data of **1** and **2** at different temperatures were extracted to generate the

Cole−Cole plots. As shown in Figures 4b and S25, in an absence of a dc field, only one process is observed between 6.0 and 20 K, while there are two semicurves in low temperature range (1.8-5.4 K), corresponding to the two relaxation processes. Therefore, their Cole−Cole plots were fitted by the generalized Debye model[33] based on eqns. 3 or 4 to extract the values and distribution of the relaxation times:

$$\chi_{ac}(\omega) = \chi_S + \frac{\chi_T - \chi_S}{1 + (i\omega\tau)^{(1-\alpha)}} \quad (3)$$

where χ_T and χ_S are the isothermal and the adiabatic susceptibility, respectively; ω is angular frequency; τ is relaxation time; α indicates deviation from a pure Debye model.[34]

$$\chi_{ac}(\omega) = \chi_{S,tot} + \frac{\Delta\chi_1}{1 + (i\omega\tau_1)^{(1-\alpha_1)}} + \frac{\Delta\chi_2}{1 + (i\omega\tau_2)^{(1-\alpha_2)}} \quad (4)$$

where $\chi_{S,tot} = \chi_{S1} + \chi_{S2}$, $\Delta\chi_1 = \chi_{T1} - \chi_{S1}$ and $\Delta\chi_2 = \chi_{T2} - \chi_{S2}$.

In contrast, the Cole-Cole plots show there is only one relaxation process under 0.15 T dc field (Figure S26), which were fitted by eqn. 3. The obtained α values at zero-field reflect a wide relaxation time distribution while the distribution become narrower with the rise of the temperature (Table S7). Under an applied dc field of 0.15 T, the α values become very small with 0.22×10^{-5} to 0.035 for **1**, which tend to zero corresponding to a single relaxation process. But for **2**, the obtained α values are still little large in the low temperature range (1.8-5.0 K) (Figure S26, Table S8).

In order to get more insight into the relaxation mechanism, we have tried to synthesize the

diluted samples with diamagnetic Zn matrix. Only diluted complex $(HNEt_3)_2[Co_{0.1}Zn_{0.9}(L^1)_2]\cdot H_2O$ (**1'**) was successfully obtained, which was confirmed by ICP and XRD data (Figure S27). The frequency- and temperature-dependent ac susceptibilities of **1'** at 0 T displays only one relaxation process under whole temperature range (Figures S28-S29), further indicating the second relaxation mechanism at low temperatures and frequencies in **1** is attributed to the interatomic interactions. The plot of $ln(\tau)$ versus T^{-1} extracted from the variable-frequency susceptibility data was fitted by the Raman process, respectively, yielding the parameters $C = 0.005(9)$ s^{-1} $K^{-4.7}$, $n = 4.7(1)$ (Figure S30). Moreover, the Cole−Cole plots (Figure S31) were also constructed by fitting of the χ_M'' versus χ_M' data by the generalized Debye model,[34] yielding the α parameters in the range of 0.58-0.04 (Table S9), which indicating a wide relaxation time distribution in low temperature region (1.8-5.5 K) but with a narrow distribution in high temperature range (6.0-19 K). In summary, the observation of slow magnetic relaxation in the diluted sample **1'** proves that the slow magnetic relaxation is intrinsic to the individual $[Co(L^1)_2]^{2-}$ molecules.

Magnetic hysteresis loops in the field-dependence of the magnetization were measured at 1.8 K with the various field sweep rates (0.06 to 0.60 T/min) and with a constant sweep rate at 0.30 T/min over the temperature range 1.8 to 3.0 K (Figures 5 and S32). A typical hysteresis loop in the field-dependent magnetization was observed for both **1** and **2**, an important characteristic of SMMs, which is rarely observed for Co^{II}-based SIMs.[8a,8b,11b-c,13g,h] The hysteresis loops are found as a function of the field sweep rate and the temperature, which becomes larger with increasing the sweep rates at 1.8 K (Figures 5 and S32, top), but smaller with increasing the temperature at a constant sweep rate of 0.30 T/min (Figures 5 and

S32, bottom), as observed in the other reported Co^{II}-based SIMs.[8a,8b,11b,c,13g,h] It is interesting that the loop is open at zero field with sweep rate range from 0.06 to 0.6 T/min at 1.8 K with a small coercity (0.007−0.010 T for **1** and 0.017−0.022 T for **2**). But at the sweep rate of 0.3 T/min, as the temperature rises, the hysteresis loops close gradually and vanish at about 3.0 K due to the fast relaxation through quantum tunneling of magnetization.

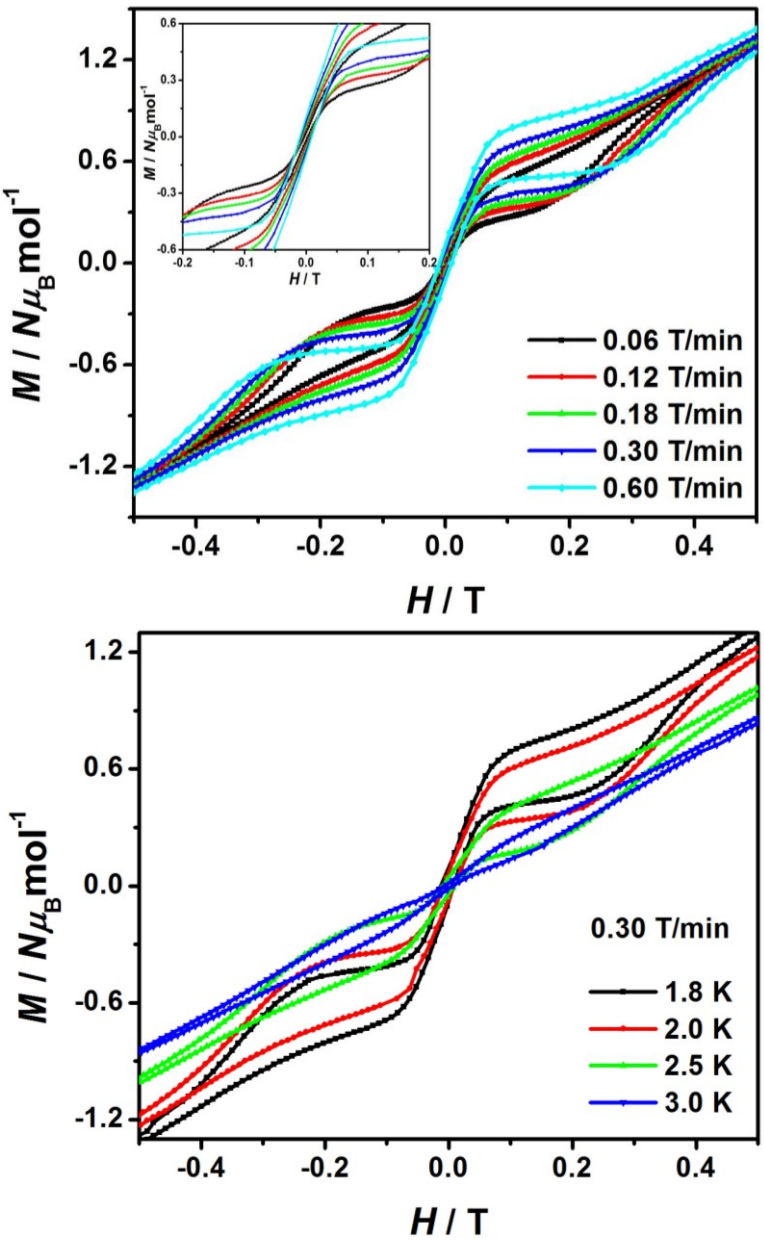

Figure 5. Magnetic hysteresis loop of **1** under various field sweep rates at 1.8 K (top) and in

the temperature range of 1.8 to 3.0 K (bottom).

Conclusions

Two four-coordinate complexes **1** and **2** with oxamide ligands have been synthesized and characterized. Both behave as single-ion magnets (SIMs) without the requirement of an applied dc field. The SIM behavior originates from the strong axial distortion induced by the oxamidate ligands, which leads to a small gap between the ground and first excited states resulting in the large magnetic anisotropy. Compared with the four-coordinate tetrahedral Co^{II}-SIMs reported by Carl[11b] and Rechkemmer[11c], which possess the small N-Co-N bite angles introduced by *N,N'*-chelating ligand (71.5°and 80.59°), our tetrahedral Co^{II} complexes exhibit similar elongated tetrahedral geometry with the similar bite angle (81.3(2)° for **1** and 83.38(12)° for **2**). Because of the similar coordination environments in **1** and **2**, the difference of the energy gap between **1** (261.7 cm^{-1}) and **2** (289.8 cm^{-1}) calculated by ab initio theoretical calculations is not likely significant. The high-performance SMM behavior in the absence of external field and a hysteresis loop at 1.8 K make **1** and **2** to be new examples for zero-field Co^{II}-based SIMs (SMMs). These two mononuclear Co(II) complexes not only enrich the family of Co^{II}-based SIMs but also help the search for new better SIMs.

ASSOCIATED CONTENT

* Supporting Information

The Supporting Information is available free of charge on the ACS Publications website at DOI:

Table for the summary of crystal data and refinement for **1** and **2**; Table for the calculations by SHAPE; Additional figures for magnetic characterization; Table for the fitting data for the Cole-Cole plots; Further theoretical calculation results; Additional structural data in CIF format (CIF).

AUTHOR INFORMATION

Corresponding Authors

Emails: xtchen@nju.edu.cn, zhangyiquan@njnu.edu.cn

Notes

The authors declare no competing financial interest.

ACKNOWLEDGMENT

We are grateful for the financial support from the National Natural Science Grant of China (No. 21471078 to XTC, 11774178 to YQZ and U1732275 to WT), the National Key Research and Development Program of China (No. 2016YFA0401802 to WT) and the US National Science Foundation (CHE-1633870 to ZLX). A portion of this work was performed on the Steady High Magnetic Field Facilities, High Magnetic Field Laboratory, CAS.

REFRENCES

(1) Sessoli, R.; Gatteschi, D.; Caneschi, A.; Novak, M. A. Magnetic bistability in a metal-ion cluster. *Nature* **1993**, *365*, 141–143.

(2) (a) Gatteschi, D.; Sessoli, R.; Villain, J. *Molecular Nanomagnets*; Oxford University Press: Oxford, **2006**. (b) Winpenny, R., Ed. *Single-Molecule Magnets and Related Phenomena*; Springer: New York, **2006**.

(3) (a) Mannini, M.; Pineider, F.; Sainctavit, P.; Danieli, C.; Otero, E.; Sciancalepore, C.; Talarico, A. M.; Arrio, M.-A.; Cornia, A.; Gatteschi, D.; Sessoli, R. Magnetic memory of a single-molecule quantum magnet wired to a gold surface. *Nat. Mater.* **2009**, *8*, 194−197. (b) Westerstroem, R.; Dreiser, J.; Piamonteze, C.; Muntwiler, M.; Weyeneth, S.; Kraemer, K.; Liu, S. X.; Decurtins, S.; Popov, A.; Yang, S.; Dunsch, L.; Greber, T. Tunneling, remanence, and frustration in dysprosium based endohedral single molecule magnets. *Phys. Rev. B.* **2014**, *89*, 060406(1-4). (c) Leuenberger, M. N.; Loss, D. Quantum computing in molecular magnets. *Nature* **2001**, *410*, 789−793. (d) Lehmann, J.; Gaita-Arino, A.; Coronado, E.; Loss, D. Spin qubits with electrically gated polyoxometalate molecules. *Nat. Nanotechnol.* **2007**, *2*, 312−317. (e) Bogani, L.; Wernsdorfer, W. Molecular spintronics using single-molecule magnets. *Nat. Mater.* **2008**, *7*, 179−186.

(4) (a) Waldmann, O. A criterion for the anisotropy barrier in single-molecule magnets. *Inorg. Chem.* **2007**, *46*, 10035–10037. (b) Neese, F.; Pantazis, D. A. What is not required to make a single molecule magnet. *Faraday Discuss.* **2011**, *148*, 229–238.

(5) Ishikawa, N.; Sugita, M.; Ishikawa, T.; Koshihara, S.-Y.; Kaizu, Y. Lanthanide double-decker complexes functioning as magnets at the single-molecular level. *J. Am. Chem. Soc.* **2003**, *125*, 8694–8695.

(6) Freedman, D. E.; Harman, W. H.; Harris, T. D.; Long, G. J.; Chang, C. J.; Long, J. R.

Slow magnetic relaxation in a high-spin iron(II) complex. *J. Am. Chem. Soc.* **2010**, *132*, 1224–1225.

(7) (a) Craig, G. A.; Murrie, M. 3d single-ion magnets. *Chem. Soc. Rev.* **2015**, *44*, 2135-2147. (b) Frost, J. M.; Harriman, K. L. M.; Murugesu, M. The rise of 3-d single-ion magnets in molecular magnetism: towards materials from molecules? *Chem. Sci.* **2016**, *7*, 2470-2491. (c) Bar, A. K.; Pichon, C.; Sutter, J.-P. Magnetic anisotropy in two- to eight-coordinated transition–metal complexes: Recent developments in molecular magnetism. *Coord. Chem. Rev.* **2016**, *308*, 346-380. (d) Feng, M.; Tong, M.-L. Single ion magnets from 3d to 5f: developments and strategies. *Chem. Eur. J.* **2018**, *24*, 7574–7594.

(8) (a) Bunting, P. C.; Atanasov, M.; Damgaard-Møller, E.; Perfetti, M.; Crassee, I.; Orlita, M.; Overgaard, J.; van Slageren, J.; Neese, F.; Long, J. R. A linear cobalt(II) complex with maximal orbital angular momentum from a non-Aufbau ground state. *Science* **2018**, *362*, eaat7319 (1-9). (b) Yao, X.–N.; Du, J.–Z.; Zhang, Y.–Q.; Leng, X.–B.; Yang, M.–W.; Jiang, S.–D.; Wang, Z.–X.; Ouyang, Z.–W.; Deng, L.; Wang, B.–W.; Gao, S. Two-coordinate Co(II) imido complexes as outstanding single-molecule magnets. *J. Am. Chem. Soc.* **2017**, *139*, 373−380. (c) Deng, Y.–F.; Wang, Z.-X.; Ouyang, Z. W.; Yin, B.; Zheng, Z.–P.; Zheng, Y.–Z. Large easy-plane magnetic anisotropy in a three-coordinate cobalt(II) complex $[Li(THF)_4][Co(NPh_2)_3]$. *Chem. Eur. J.* **2016**, *22*, 14821– 4825.

(9) (a) Zadrozny, J. M.; Liu, J.; Piro, N. A.; Chang, C. J.; Hill, S.; Long, J. R. Slow magnetic relaxation in a pseudotetrahedral cobalt(II) complex with easy-plane

anisotropy. *Chem. Commun.* **2012**, *48*, 3927−3929. (b) Gomez-Coca, S.; Cremades, E.; Aliaga- Alcalde, N.; Ruiz, E. Mononuclear single-molecule magnets: tailoring the magnetic anisotropy of first-row transition-metal complexes. *J. Am. Chem. Soc.* **2013**, 135, 7010-7018. (c) Boča, R.; Miklovič, J.; Titiš, J. Simple mononuclear cobalt(II) complex: a single-molecule magnet showing two slow relaxation processes. *Inorg. Chem.* **2014**, *53*, 2367–2369. (d) Saber. M. R.; Dunbar. K. R. Ligands effects on the magnetic anisotropy of tetrahedral cobalt complexes. *Chem. Commun.* **2014**, *50*, 12266-12269.

(10) (a) Zadrozny, J. M.; Long, J. R. Slow magnetic relaxation at zero field in the tetrahedral complex $[Co(SPh)_4]^{2-}$. *J. Am. Chem. Soc.* **2011**, *133*, 20732−20734. (b) Zadrozny, J.; M., Telser, J.; Long, J. R. Slow magnetic relaxation in the tetrahedral cobalt(II) complexes $Co(EPh)_4^{2-}$ (E = O, S, Se). *Polyhedron*. **2013**, *64*, 209–217. (c) Fataftah, M. S., Zadrozny, J. M., Rogers, D. M.; Freedman, D. E. A mononuclear transition metal single-molecule magnet in a nuclear spin-free ligand environment. *Inorg. Chem.* **2014**, *53*, 10716–10721. (d) Vaidya, S.; Tewary, S.; Singh, S. K.; Langley, S. K.; Murray, K. S.; Lan, Y.; Wernsdorfer, W.; Rajaraman, G.; Shanmugam, M. What Controls the Sign and Magnitude of Magnetic Anisotropy in Tetrahedral Cobalt(II) Single-Ion Magnets? *Inorg. Chem.* **2016**, *55*, 9564−9578. (e) Yao, X.–N.; Yang, M. W.; Xiong, J.; Liu, J.–J.; Gao, Chen.; Meng, Y.-S.; Jiang, S.-D.; Wang, B.-W.; Gao, S. Enhanced magnetic anisotropy in a telluriumcoordinated cobalt single-ion magnet. *Inorg. Chem. Front.* **2017**, *4*, 701–705. (f) Suturina, E. A.; Nehrkorn, J.; Zadrozny, J. M.; Liu, J.; Atanasov, M.; Weyhermüller, T.; Maganas, D.;

Hill, S.; Schnegg, A.; Bill, E.; Long, J. R.; Neese, F. Magneto-structural correlations in pseudotetrahedral forms of the $[Co(SPh)_4]^{2-}$ complex probed by magnetometry, MCD spectroscopy, advanced EPR techniques, and ab initio electronic structure calculations. *Inorg. Chem.* **2017**, *56*, 3102-3118.

(11) (a) Vallejo, J.; Pardo, E.; Viciano-Chumillas, M.; Castro, I.; Amorós, P.; Déniz, M.; Ruiz-Pérez, C.; Yuste-Vivas, C.; Krzystek, J.; Julve, M.; Lloreta, F.; Cano, J. Reversible solvatomagnetic switching in a single-ion magnet from an entatic state. *Chem. Sci.* **2017**, *8*, 3694-3702. (b) Carl, E.; Demeshko, S.; Meyer, F.; Stalke, D. Triimidosulfonates as acute bite-angle chelates: slow relaxation of the magnetization in zero field and hysteresis loop of a Co^{II} complex. *Chem. Eur. J.* **2015**, *21*, 10109–10115. (c) Rechkemmer,Y.; Breitgoff, F. D.; van der Meer, M.; Atanasov, M.; Hakl, M.; Orlita, M.; Neugebauer, P.; Neese, F.; Sarkar, B.; van Slageren, J. A four-coordinate cobalt(II) single-ion magnet with coercivity and a very high energy barrier. *Nat. Commun.* **2016**, *7*, 10467(1-8).

(12) Piecha-Bisiorek, A.; Bieńko, A.; Jakubas, R.; Boča, R.; Weselski, M.; Kinzhybalo, V.; Pietraszko, A.; Wojciechowska, M.; Medycki, W.; Kruk, D. Physical and structural characterization of imidazolium-based organic–inorganic hybrid: $(C_3N_2H_5)_2[CoCl_4]$. *J. Phys. Chem. A*. **2016**, *120*, 2014-2021.

(13) (a) Rajnák, C.; Titiš, J.; Fuhr, O.; Ruben, M.; Boča, R. Single-molecule magnetism in a pentacoordinate cobalt(II) complex supported by an antenna ligand. *Inorg. Chem.* **2014**, *53*, 8200−8202. (b) Jurca, T.; Farghal, A.; Lin, P. H.; Korobkov, I.; Murugesu, M.; Richeson, D. S. Single-molecule magnet behavior with a single metal center

enhanced through peripheral ligand modifications. *J. Am. Chem. Soc.* **2011**, *133*, 15814–15817. (c) Vallejo, J.; Castro, I.; Ruiz-García, R.; Cano, J.; Julve, M.; Lloret, F.; De Munno, G.; Wernsdorfer, W.; Pardo, E. Field-induced slow magnetic relaxation in a six- coordinate mononuclear cobalt(II) complex with a positive anisotropy. *J. Am. Chem. Soc.* **2012**, *134*, 15704−15707. (d) Gómez-Coca, S.; Urtizberea, A.; Cremades, E.; Alonso, P. J.; Camón, A.; Ruiz, E.; Luis, F. Origin of slow magnetic relaxation in kramers ions with non-uniaxial anisotropy. *Nat. Commun.* **2014**, *5*, 4300 (1-8). (e) Novikov, V. V.; Pavlov, A. A.; Nelyubina, Y. V.; Boulon, M. E.; Varzatskii, O. A.; Voloshin, Y. Z.; Winpenny, R. E. P. A trigonal prismatic mononuclear cobalt(II) complex showing single-molecule magnet behavior. *J. Am. Chem. Soc.* **2015**, 137, 9792-9795. (f) Zhu, Y.-Y.; Zhu, M.-S.; Yin, T.-T.; Meng, Y.-S.; Wu, Z.-Q.; Zhang, Y.-Q.; Gao, S. Cobalt(II) coordination polymer exhibiting single-ion-magnet-type field-induced slow relaxation behavior. *Inorg. Chem.* **2015**, *54*, 3716−3718. (g) Pavlov, A. A.; Nelyubina, Y. V.; Kats, S. V.; Penkova, L. V.; Efimov, N. N.; Dmitrienko, A. O.; Vologzhanina, A. V.; Belov, A. S.; Voloshin, Y. Z.; Novikov, V. V. Polymorphism in a cobalt-based single-ion magnet tuning its barrier to magnetization relaxation. *J. Phys. Chem. Lett.* **2016**, *7*, 4111−4116. (h) Yao, B.; Deng, Y.-F.; Li, T.; Xiong, J.; Wang, B.-W.; Zheng, Z.; Zhang, Y.-Z. Construction and Magnetic Study of a Trigonal-Prismatic Cobalt(II) Single-Ion Magnet. *Inorg. Chem.*, **2018**, *57*, 14047−14051. (i) Moseley, D. H.; Stavretis, S. E.; Thirunavukkuarasu, K.; Ozerov, M.; Cheng, Y.; Daemen, L. L.; Ludwig, J.; Lu, Z.; Smirnov, D.; Brown, C. M.; Pandey, A.; Ramirez-Cuesta, A. J.; Lamb, A. C.; Atanasov, M.; Bill, E.; Neese, F.; Xue, Z.-L.

Spin–Phonon Couplings in Transition Metal Complexes with Slow Magnetic Relaxation. *Nat. Commun.* **2018**, *9*, 2572 (1-11).

(14) (a) Chen, L.; Cui, H.-H.; Stavretis, S. E.; Hunter, S. C.; Zhang, Y.-Q.; Chen, X.-T.; Sun, Y. -C.; Wang, Z.- X.; Song, Y.; Podlesnyak, A. A.; Ouyang, Z.W.; Xue, Z.-L. Slow Magnetic Relaxations in Cobalt(II) Tetranitrate Complexes. Studies of magnetic anisotropy by inelastic neutron scattering and high-frequency and high-field EPR spectroscopy. *Inorg. Chem.* **2016**, *55*, 12603−12617. (b) Chen, L.; Wang, J.; Wei, J.–M.; Wernsdorfer, W.; Chen, X.–T.; Zhang, Y.–Q.; Song, Y.; Xue, Z.–L. Slow magnetic relaxation in a mononuclear eight-coordinate cobalt(II) complex. *J. Am. Chem. Soc.* **2014**, *136*, 12213−12216.

(15) Gatteschi, D.; Sessoli, R. Quantum tunneling of magnetization and related phenomena in molecular materials. *Angew. Chem., Int. Ed.* **2003**, *42*, 268−297.

(16) Maulding, D. R.; Clarke, R. A.; Roberts, B. G.; Rauhut, M. M. Chemiluminescence from reactions of electrophilic oxamides with hydrogen peroxide and fluorescent compounds. *J. Org. Chem.* **1968**, *33*, 250-254.

(17) Cotton, F. A.; Liu, C. Y.; Murillo, C. A.; Villagran, D.; Wang, X. P. Modifying electronic communication in dimolybdenum units by linkage isomers of bridged oxamidate dianions. *J. Am. Chem. Soc.* **2003**, *125*, 13564-13575.

(18) SMART & SAINT Software Reference Manuals, version 6.45; Bruker Analytical X-ray Systems, Inc.: Madison, WI, **2003**.

(19) SAINT, Program for Data Extraction and Reduction, Siemens Analytical X-ray Instruments, Madison, WI, 1994–1996.

(20) Sheldrick, G. M. SADABS: Software for Empirical Absorption Correction, version 2.05; University of Göttingen: Göttingen, Germany, **2002**.

(21) Sheldrick, G. M. SHELXL14: Program for Crystal Structure Refinement; University of Göttingen: Göttingen, Germany, **2014**.

(22) Bain, G. A.; Berry, J. F. Diamagnetic corrections and Pascal's constants. *J. Chem. Educ.* **2008**, *85*, 532-536.

(23) Fernández, I.; Pedro, J. R.; Roselló, A. L.; Ruiz, R.; Castro, I.; Ottenwaelder, X.; Journaux, Y. *Eur. J. Org. Chem.* **2001**, 1235-1247.

(24) (a) Banci, L.; Bencini, A.; Benelli, C.; Gatteschi, D.; Zanchini, C. Spectral-structural correlations in high-spin cobalt(II) complexes. *Struct. Bond.* **1982**, *52*, 37–86.. (b) Zadrozny, J. M.; Telser, J.; Long, J. R. *Polyhedron* **2013**, *64*, 209-217.

(25) Dou, Y. S. Equations for calculating *Dq* and *B*. *J. Chem. Educ.* **1990**, *67*, 134.

(26) Parsons, S.; White, D.; Tasker, P.; Wood, P. A. *CSD Communication (Private Communication)* **2004**.

(27) (a) Llunell, M.; Casanova, D.; Cirera, J.; Alemany, P.; Alvarez, S. Shape Program, Version 2.1, **2013**. (b) Alvarez, S.; Alemany, P.; Casanova, D.; Cirera, J.; Llunell, M.; Avnir, D. Shape maps and polyhedral interconversionpaths in transition metal chemistry. *Coord. Chem. Rev.* **2005**, 249, 1693-1708.

(28) Chilton, N. F.; Anderson, R. P.; Turner, L. D.; Soncini, A.; Murray, K. S. PHI: A Powerful New Program for the Analysis of Anisotropic Monomeric and Exchange-Coupled Polynuclear d- and f-Block Complexes. *J. Comput. Chem.* **2013**, *34*, 1164−1175.

(29) (a) Granovsky, A. A. Extended multi-configuration quasi-degenerate perturbation theory: The new approach to multi-state multi-reference perturbation theory. *J. Chem. Phys*. **2011**, *134*, 214113. (b) Shiozaki, T.; Gyorffy, W.; Celani, P.; Werner, H. -J. Communication: Extended multi-state complete active space second-order perturbation theory: Energy and nuclear gradients. *J. Chem. Phys*. **2011**, *135*, 081106. (c) Ungur, L.; Chibotaru, L. F. Ab initio crystal field for lanthanides. *Chem. Eur. J.* **2017**, *23*, 3708-3718.

(30) Aquilante, F.; Autschbach, J.; Carlson, R. K.; Chibotaru, L. F.; Delcey, M. G.; De Vico, L.; Fdez. Galván, I.; Ferré, N.; Frutos, L. M.; Gagliardi, L.; Garavelli, M.; Giussani, A.; Hoyer, C. E.; Li Manni, G.; Lischka, H.; Ma, D.; Malmqvist, P. Å.; Müller, T.; Nenov, A.; Olivucci, M.; Pedersen, T. B.; Peng, D.; Plasser, F.; Pritchard, B.; Reiher, M.; Rivalta, I.; Schapiro, I.; Segarra- Martí, J.; Stenrup, M.; Truhlar, D. G.; Ungur, L.; Valentini, A.; Vancoillie, S.; Veryazov, V.; Vysotskiy, V. P.; Weingart, O.; Zapata, F.; Lindh, R. MOLCAS 8: New Capabilities for Multiconfigurational Quantum Chemical Calculations across the Periodic Table. *J. Comput. Chem*. **2016**, *37*, 506-541.

(31) Ungur, L.; Chibotaru, L. F. Strategies toward high-temperature lanthanide-based single-molecule magnets. *Inorg. Chem.* **2016**, *55*, 10043-10056.

(32) (a) Carlin R. L.; van Duyneveldt, A. J. *Magnetic Properties of Transition Metal compounds*; Springer-Verlag: New York, 1976. (*b*) Shrivastava, K.N. Theory of spin-lattice relaxation, *Phys. Status Solidi B* **1983**, *117*, 437-458.

(33) (a) Cole, K. S.; Cole, R. H. Dispersion and absorption in dielectrics I. Alternating current characteristics. *J. Chem. Phys.* **1941**, *9*, 341−351. (b) Guo, Y.-N.; Xu, G.-F.;

Guo, Y.; Tang, J. Relaxation dynamics of dysprosium(III) single molecule magnets. *Dalton Trans.* **2011**, *40*, 9953−9963.

For Table of Contents only

Two mononuclear tetrahedral Co(II) complexes display hysteresis loop as well as slow magnetic relaxation in the absence of an applied dc field.